

October 2, 2015

Excited-state energies and scattering phase shifts from lattice QCD with the stochastic LapH method

COLIN MORNINGSTAR^{1, a} JOHN BULAVA,^b BRENDAN FAHY,^c JACOB FALLICA,^a
ANDREW HANLON,^d BEN HÖRZ,^b KEISUKE JUGE,^e CHIK HIM WONG^f

^a *Dept. of Physics, Carnegie Mellon University, Pittsburgh, PA 15213, USA*

^b *School of Mathematics, Trinity College, Dublin 2, Ireland*

^c *High Energy Accelerator Research Organization (KEK), Ibaraki 305-0801, Japan*

^d *Dept. of Physics and Astronomy, Univ. of Pittsburgh, Pittsburgh, PA 15260, USA*

^e *Dept. of Physics, University of the Pacific, Stockton, CA 95211, USA*

^f *Dept. of Physics, University of Wuppertal, Gausstrasse 20, D-42119, Germany*

Recent results in computing excited-state energies and meson-meson scattering phase shifts in lattice QCD are presented. A stochastic method of treating the low-lying modes of quark propagation that exploits Laplacian Heaviside quark-field smearing makes such studies possible now on large $32^3 \times 256$ and $48^3 \times 128$ lattices at near physical pion masses. Levels are identified using a variety of probe interpolating operators, which include both single-hadron and a large number of two-hadron operators.

PRESENTED AT

Twelfth Conference on the Intersections of Particle
and Nuclear Physics (CIPANP 2015),
Vail, CO, USA, May 19–24, 2015

¹Presenter

1 Introduction

In a series of papers[1, 2, 3, 4, 5, 6], we have been striving to compute the finite-volume stationary-state energies of QCD using Markov-chain Monte Carlo integration of the QCD path integrals formulated on a space-time lattice. In this talk, we report on results in the zero-momentum bosonic $I = 1$, $S = 0$, T_{1u}^+ symmetry sector of QCD obtained on a large $32^3 \times 256$ anisotropic lattice for which the pion mass is around 240 MeV. All needed Wick contractions are efficiently evaluated using a stochastic method[5] of treating the low-lying modes of quark propagation that exploits Laplacian Heaviside quark-field smearing. Given the large number of levels extracted, level identification becomes a key issue. We also use a variety of two-pion energies in finite volume with different total momenta to calculate the P -wave scattering phase shifts in the $I = 1$ channel, and extract the mass and width of the ρ resonance. The scattering phase shifts are also obtained on a $48^3 \times 128$ isotropic lattice.

2 Operators, configurations, and analysis

The stationary-state energies in a particular symmetry sector can be extracted from an $N \times N$ Hermitian correlation matrix $\mathcal{C}_{ij}(t) = \langle 0 | O_i(t+t_0) \bar{O}_j(t_0) | 0 \rangle$, where the N operators \bar{O}_j act on the vacuum to create the states of interest at source time t_0 and are accompanied by conjugate operators O_i that can annihilate these states at a later time $t + t_0$. Estimates of $\mathcal{C}_{ij}(t)$ are obtained with the Monte Carlo method using the stochastic LapH method[5] which allows all needed quark-line diagrams to be computed.

All of our single-hadron operators are assemblages of basic building blocks which are gauge-covariantly-displaced, LapH-smearred quark fields, as described in Refs. [1, 5, 6]. Each of our single-hadron operators creates and annihilates a definite momentum. Group-theoretical projections are used to construct operators that transform according to the irreducible representations of the space group O_h^1 , plus G -parity, when appropriate. In order to build up the necessary orbital and radial structures expected in the hadron excitations, we use a variety of spatially-extended configurations. For practical reasons, we restrict our attention to certain classes of momentum directions for the single hadron operators: on axis $\pm\hat{x}$, $\pm\hat{y}$, $\pm\hat{z}$, planar diagonal $\pm\hat{x} \pm \hat{y}$, $\pm\hat{x} \pm \hat{z}$, $\pm\hat{y} \pm \hat{z}$, and cubic diagonal $\pm\hat{x} \pm \hat{y} \pm \hat{z}$. However, some special momentum directions, such as $\pm 2\hat{x} \pm \hat{y}$, are used. We construct our two-hadron operators as superpositions of single-hadron operators of definite momenta. Again, group-theoretical projections are employed to produce two-hadron operators that transform irreducibly under the symmetry operations of our system. This approach is efficient for creating large numbers of two-hadron operators, and generalizes to three or more hadrons.

In finite volume, all energies are discrete so that each correlator matrix element has a spectral representation of the form

$$\mathcal{C}_{ij}(t) = \sum_n Z_i^{(n)} Z_j^{(n)*} e^{-E_n t}, \quad Z_j^{(n)} = \langle 0 | O_j | n \rangle, \quad (1)$$

assuming temporal wrap-around (thermal) effects are negligible. We extract energies from our correlation matrices using a “single rotation” or “fixed coefficient” method. Starting with a raw correlation matrix $\mathcal{C}(t)$, we first try to remove the effects of differing normalizations by forming the matrix $C_{ij}(t) = \mathcal{C}_{ij}(t) (\mathcal{C}_{ii}(\tau_N) \mathcal{C}_{jj}(\tau_N))^{-1/2}$, taking τ_N at a very early time, such as $\tau_N = 3$. We ensure that C is positive definite and has a reasonable condition number. Standard projection methods can be used to remove problematic modes. We then solve the generalized eigenvector problem $Ax = \lambda Bx$ with $A = C(\tau_D)$ and $B = C(\tau_0)$ for particular choices of times τ_0 and τ_D (see below). The eigenvectors obtained are used to “rotate” the correlator $C(t)$ into a correlator $G(t)$ for which $G(\tau_0) = 1$, the identity matrix, and $G(\tau_D)$ is diagonal. At other times, $G(t)$ need not be diagonal. However, with judicious choices of τ_0 and τ_D , one finds that the off-diagonal elements of $G(t)$ remain zero within statistical precision for $t > \tau_D$. The rotated correlator is given by

$$G(t) = U^\dagger C(\tau_0)^{-1/2} C(t) C(\tau_0)^{-1/2} U, \quad (2)$$

where the columns of U are the orthonormalized eigenvectors of the matrix given by $C(\tau_0)^{-1/2} C(\tau_D) C(\tau_0)^{-1/2}$. Rotated effective masses can then be defined by

$$m_G^{(n)}(t) = \frac{1}{\Delta t} \ln \left(\frac{G_{nn}(t)}{G_{nn}(t + \Delta t)} \right), \quad (3)$$

which tend to the lowest-lying N stationary-state energies produced by the N operators, as long as the off-diagonal elements of the rotated correlator matrix remain consistent with zero. Correlated- χ^2 fits to the estimates of $G_{nn}(t)$ using the forms

$$A_n e^{-E_n t} \left(1 + B_n e^{-\Delta_n^2 t} \right) + A_n e^{-E_n (T-t)} \left(1 + B_n e^{-\Delta_n^2 (T-t)} \right), \quad (4)$$

where T is the temporal extent of the lattice, yield the energies E_n and the overlaps A_n to the rotated operators for each n . Using the rotation coefficients, one can then easily obtain the overlaps $Z_j^{(n)} = C(\tau_0)_{jk}^{1/2} U_{kn} A_n$ (no summation over n) corresponding to the rows and columns of the correlation matrix $C(t)$.

Here, we present results obtained using a set of 412 gauge-field configurations on a large $32^3 \times 256$ anisotropic lattice with a pion mass $m_\pi \sim 240$ MeV. We refer to this ensemble as the $(32^3|240)$. These ensembles were generated using the Rational Hybrid Monte Carlo (RHMC) algorithm[7]. In each ensemble, successive configurations are separated by 20 RHMC trajectories to minimize autocorrelations. An improved

anisotropic clover fermion action and an improved gauge field action are used[8]. In these ensembles, $\beta = 1.5$ and the s quark mass parameter is set to $m_s = -0.0743$ in order to reproduce a specific combination of hadron masses[8]. The light quark mass parameters are set to $m_u = m_d = -0.0860$, resulting in a pion mass around 240 MeV. The spatial grid size is $a_s \sim 0.12$ fm, whereas the temporal spacing is $a_t \sim 0.035$ fm.

In our operators, a stout-link[9] staple weight $\xi = 0.10$ is used with $n_\xi = 10$ iterations. For the cutoff in the LapH smearing, we use $\sigma_s^2 = 0.33$, which translates into the number N_v of LapH eigenvectors retained being $N_v = 264$ for our 32^3 lattice. We use Z_4 noise in all of our stochastic estimates of quark propagation. Our variance reduction procedure is described in Ref. [5]. On the 32^3 lattices, we use 8 widely-separated source times t_0 .

3 Energies in the T_{1u}^+ channel

We focus here on the resonance-rich $I = 1$, $S = 0$, T_{1u}^+ channel of total zero momentum. This channel has odd parity, even G -parity, and contains the spin-1 and spin-3 mesons. Low statistics runs on smaller lattices led us to include 14 particular single-meson (quark-antiquark) operators. We took special care to include operators that could produce the spin-3 $\rho_3(1690)$ state, in addition to the other spin-1 states. Low statistics runs also gave us the masses of the lowest-lying mesons, such as the π, η, K , and so on. Given these known mesons, we used software written in MAPLE to find all possible two-meson states in our cubic box in this T_{1u}^+ symmetry channel, assuming no energy shifts from interactions or the finite volume. We used these so-called “expected two-meson levels” to guide our choice of two-meson operators to include. We included 23 isovector-isovector meson operators, 31 operators that combine an isovector with a light isoscalar (using only u, d quarks), 31 operators that combine an isovector with an $\bar{s}s$ isoscalar meson, and 9 kaon-antikaon operators.

We obtained results for the lowest 50 energy levels using the $(32^3|240)$ ensemble from our 108×108 correlation matrix. The rotated effective masses $m_G^{(n)}(t)$ (see Eq. (3)) using $\tau_0 = 5$ and $\tau_D = 8$ are shown for the first 25 levels in Fig. 1. The results shown here are not finalized yet. We are still varying the fitting ranges to improve the χ^2 , as needed in some instances. We are investigating the effects of adding more operators, and we are even still verifying our analysis/fitting software. However, these figures do demonstrate that the extraction of a large number of energy levels is indeed possible, and the plots indicate the level of precision that can be attained with our stochastic LapH method. Keep in mind that we have not included any three-meson operators in our correlation matrix.

With such a large number of energies extracted, level identification becomes a key issue. QCD is a complicated interacting quantum field theory, so characterizing its stationary states in finite volume is not likely to be done in a simple way. Level

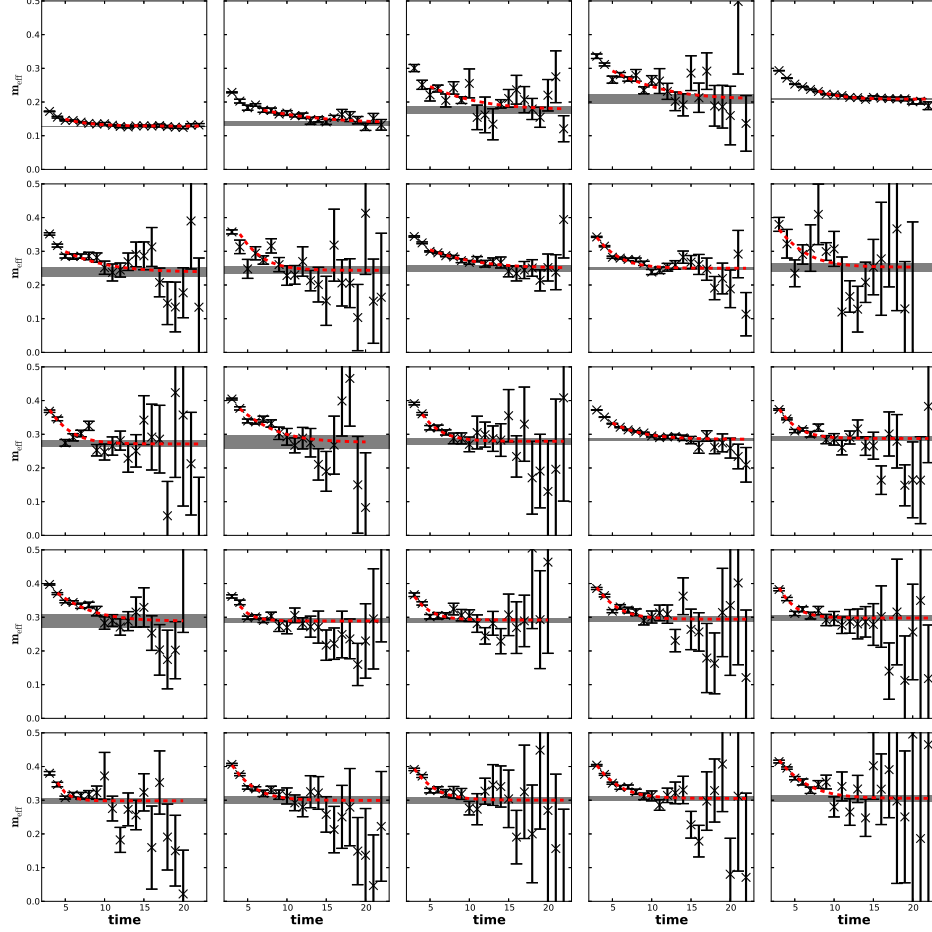


Figure 1: Rotated effective masses $m_G^{(n)}(t)$ (see Eq. (3)) for the 25 lowest-lying energy levels in the zero-momentum bosonic $I = 1$, $S = 0$, T_{1u}^+ channel for the $(32^3|240)$ ensemble using 14 single-meson operators, 23 isovector+isovector operators, 31 light-isoscalar+isovector operators, 31 $\bar{s}s$ -isoscalar+isovector operators, and 9 kaon+antikaon operators. Dashed lines indicate energy extractions from correlated- χ^2 fits. Gray bands show the best fit values of the energies, whose standard deviations are indicated by the width of each band.

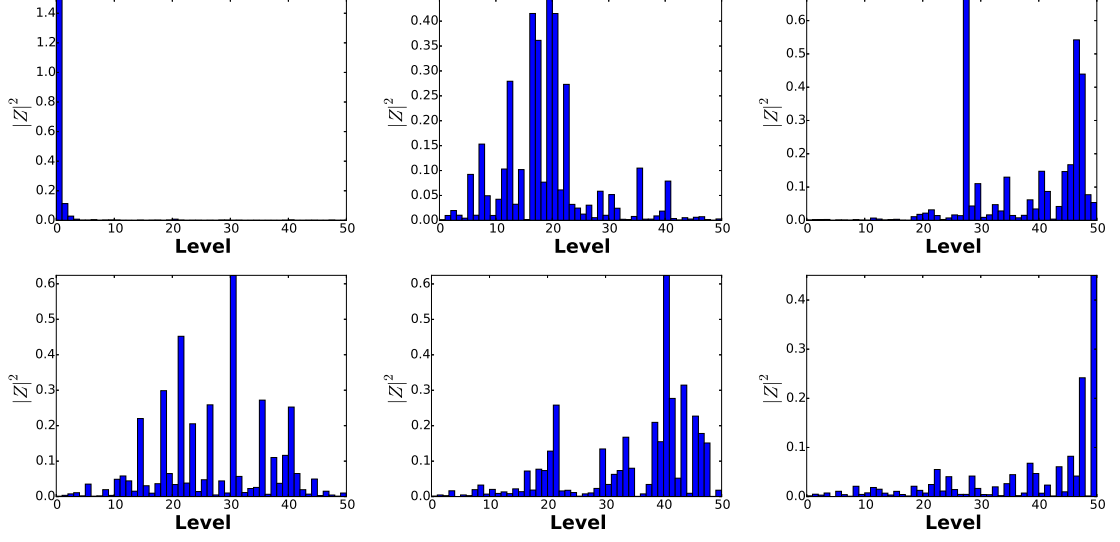


Figure 2: Overlaps $|\tilde{Z}_j^{(n)}|^2$ of “optimized” single-hadron operator \tilde{O}_j against the eigenstates labelled by n . The overall normalization is arbitrary in each plot.

identification must be inferred from the Z overlaps of our probe operators, analogous to deducing resonance properties from scattering cross sections in experiments. Judiciously chosen probe operators, constructed from smeared fields, should excite the low-lying states of interest, with hopefully little coupling to unwanted higher-lying states, and help with classifying the levels extracted. Small- a classical expansions can help to characterize the probe operators, and hence, the states they produce.

We particularly wish to identify the finite-volume stationary-state levels expected to evolve into the single-meson resonances corresponding to quark-antiquark excitations in infinite volume. To accomplish this, we utilize “optimized” single-hadron operators as our probes. We first restrict our attention to the 14×14 correlator matrix involving only the 14 chosen single-hadron operators. We then perform an optimization rotation to produce so-called “optimized” single-hadron (SH) operators \tilde{O}_j , which are linear combinations of the 14 original operators, determined in a manner analogous to Eq. (2). We order these SH-optimized operators according to their effective mass plateau values, then evaluate the overlaps $\tilde{Z}_j^{(n)}$ for these SH-optimized operators using our analysis of the full 108×108 correlator matrix. The results are shown in Fig. 2.

Our energies in the T_{1u}^+ channel are summarized by the “staircase” plot in Fig. 3. For each SH optimized operator, the level with the largest overlap is identified on this plot using a solid blue box. Other levels with significant overlaps with the SH optimized operator are indicated by boxes with a dark blue outline. The remaining

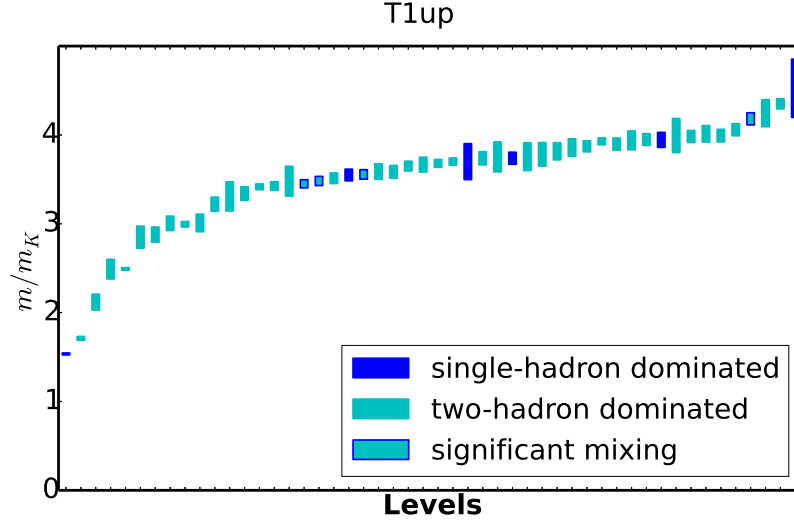


Figure 3: Energies m as ratios of the kaon mass m_K for the first fifty states excited by our single- and two-hadron operators in the T_{1u}^+ channel. For each optimized single-hadron operator, the level of maximum overlap is indicated by a solid blue box, and levels with overlaps greater than 75% of the largest are indicated by a dark blue outline.

cyan boxes are levels with overlaps dominated by two-meson operators. The energies of the levels with solid blue boxes are collected and shown in Fig. 4, which compares these energies to experiment. The finite-volume energies should agree with experiment only within the widths of the infinite-volume resonances. We believe we have extracted all meson resonances that are quark-antiquark excitations. One observes more levels in experiment, although the experimental observations are controversial in some cases. Keep in mind that resonances that are not quark-antiquark excitations, such as so-called molecular states, would not be identified by our SH optimized operator overlaps. Again, we mention that three and four meson states are not taken into account at all.

4 Scattering phase shifts from finite-volume stationary state energies

The idea that finite-volume energies can be related to infinite-volume scattering processes is actually rather old, dating back to Refs. [10, 11] in the mid-1950s. Details on how to utilize such relationships in lattice QCD were first spelled out in Refs. [12, 13]. These calculations were later revisited using an entirely field theoretic approach in Ref. [14], and subsequent works have generalized their results to treat multi-channels

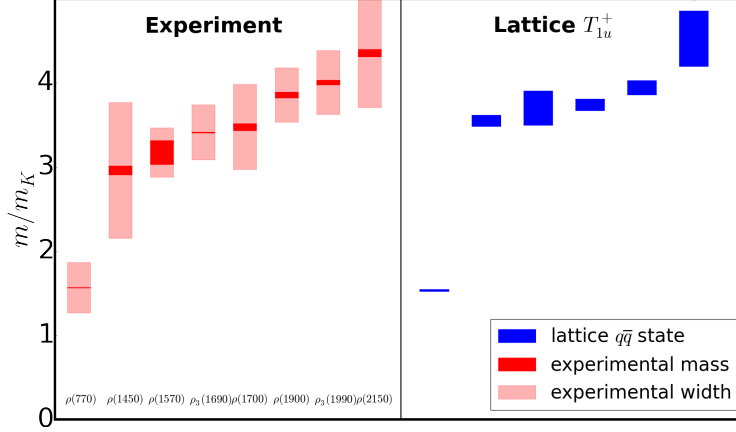


Figure 4: Comparison of the experimental spectrum of resonances with our finite-volume energies corresponding to quark-antiquark excitations. All masses m are shown as ratios over the kaon mass m_K . In the left hand side, dark red boxes indicate the experimental masses, with the vertical heights showing the uncertainties in the mass measurements. The light red boxes indicate the experimental widths of the resonances. In the right hand side, our masses for the quark-antiquark excitations are shown by dark blue boxes, whose heights indicate statistical uncertainties only. This T_{1u}^+ channel includes both ρ (spin 1) and ρ_3 (spin 3) states.

with different particle masses and nonzero spins.

For a given total momentum $\mathbf{P} = (2\pi/L)\mathbf{d}$ in a spatial L^3 volume with periodic boundary conditions, where \mathbf{d} is a vector of integers, we determine the total energy E in the lab frame for a particular two-particle interacting state in our lattice QCD simulations. If the masses of the two particles are m_1 and m_2 , we then boost to the center-of-mass frame and define the following quantities:

$$\begin{aligned}
 E_{\text{cm}} &= \sqrt{E^2 - \mathbf{P}^2}, & \gamma &= \frac{E}{E_{\text{cm}}}, & \mathbf{q}_{\text{cm}}^2 &= \frac{1}{4}E_{\text{cm}}^2 - \frac{1}{2}(m_1^2 + m_2^2) + \frac{(m_1^2 - m_2^2)^2}{4E_{\text{cm}}^2}, \\
 u^2 &= \frac{L^2 \mathbf{q}_{\text{cm}}^2}{(2\pi)^2}, & \mathbf{s} &= \left(1 + \frac{(m_1^2 - m_2^2)}{E_{\text{cm}}^2}\right) \mathbf{d}.
 \end{aligned} \tag{5}$$

The relationship between the finite-volume two-particle energy E and the infinite-volume scattering amplitudes (and phase shifts) is encoded in the matrix equation:

$$\det[1 + F^{(\mathbf{s}, \gamma, u)}(S - 1)] = 0, \tag{6}$$

where S is the usual S -matrix whose elements can be written in terms of the scattering phase shifts, and the F matrix is given in the JLS basis states by

$$F_{J'm_J L' S' a'; J m_J L S a}^{(\mathbf{s}, \gamma, u)} = \frac{\rho_a}{2} \delta_{a'a} \delta_{S'S} \left\{ \delta_{J'J} \delta_{m_J' m_J} \delta_{L'L} \right.$$

$$+W_{L'm_{L'}; Lm_L}^{(\mathbf{s}, \gamma, u)} \langle J'm_{J'} | L'm_{L'}, Sm_S \rangle \langle Lm_L, Sm_S | Jm_J \rangle \Big\}, \quad (7)$$

where J, J' refer to total angular momentum, L, L' are total orbital angular momenta, S, S' refer to total intrinsic spin in the above equation, a, a' label channels, $\rho_a = 1$ for distinguishable particles and $\rho_a = \frac{1}{2}$ for identical particles, and

$$W_{L'm_{L'}; Lm_L}^{(\mathbf{s}, \gamma, u)} = \frac{2i}{\pi\gamma u^{l+1}} \mathcal{Z}_{lm}(\mathbf{s}, \gamma, u^2) \int d^2\Omega Y_{L'm_{L'}}^*(\Omega) Y_{lm}^*(\Omega) Y_{Lm_L}(\Omega). \quad (8)$$

Notice that $F^{(\mathbf{s}, \gamma, u)}$ is diagonal in channel space, but mixes different total angular momentum sectors, whereas S is diagonal in angular momentum, but has off-diagonal elements in channel space. Also, the matrix elements of $F^{(\mathbf{s}, \gamma, u)}$ depend on the total momentum \mathbf{P} through \mathbf{s} , whereas the matrix elements of S do not. The Rummukainen-Gottlieb-Lüscher (RGL) shifted zeta functions are evaluated using

$$\begin{aligned} \mathcal{Z}_{lm}(\mathbf{s}, \gamma, u^2) &= \sum_{\mathbf{n} \in \mathbb{Z}^3} \frac{\mathcal{Y}_{lm}(\mathbf{z})}{(\mathbf{z}^2 - u^2)} e^{-\Lambda(\mathbf{z}^2 - u^2)} + \delta_{l0} \gamma \pi e^{\Lambda u^2} \left(2u D(u\sqrt{\Lambda}) - \Lambda^{-1/2} \right) \\ &+ \frac{i^l \gamma}{\Lambda^{l+1/2}} \int_0^1 dt \left(\frac{\pi}{t} \right)^{l+3/2} e^{\Lambda t u^2} \sum_{\substack{\mathbf{n} \in \mathbb{Z}^3 \\ \mathbf{n} \neq 0}} e^{\pi i \mathbf{n} \cdot \mathbf{s}} \mathcal{Y}_{lm}(\mathbf{w}) e^{-\pi^2 \mathbf{w}^2 / (t\Lambda)}, \end{aligned} \quad (9)$$

where $\mathbf{z} = \mathbf{n} - \gamma^{-1}[\frac{1}{2} + (\gamma - 1)s^{-2}\mathbf{n} \cdot \mathbf{s}]\mathbf{s}$ and $\mathbf{w} = \mathbf{n} - (1 - \gamma)s^{-2}\mathbf{s} \cdot \mathbf{n}\mathbf{s}$, the spherical harmonic polynomials are given by $\mathcal{Y}_{lm}(\mathbf{x}) = |\mathbf{x}|^l Y_{lm}(\hat{\mathbf{x}})$, and $D(x)$ is the Dawson function, defined by

$$D(x) = e^{-x^2} \int_0^x dt e^{t^2}. \quad (10)$$

We choose $\Lambda \approx 1$, although the final answer is independent of this choice. Choosing Λ near unity allows sufficient convergence speed of the summations. Gauss-Legendre quadrature is used to perform the integral, and the Dawson function is evaluated using a Rybicki approximation.

The scattering processes we study conserve both total angular momentum J and the projection of total angular momentum, say M_J . Given orthonormal states, then the unitarity of the S -matrix tells us that

$$\langle J'm_{J'} L'S'a' | S | Jm_J L S a \rangle = \delta_{J'J} \delta_{m_{J'}m_J} s_{L'S'a', LSa}^{(J)}(E), \quad (11)$$

where a', a denote other defining quantum numbers, such as channel, and $s^{(J)}$ is a unitary matrix that is independent of m_J due to rotational invariance. If the two particles have zero spin $s_1 = s_2 = 0$ and there is only one channel, then

$$s^{(J)} = s^{(L)} = e^{2i\delta_L(E)}, \quad (12)$$

\mathbf{d}	Λ	$\cot \delta_1$
(0,0,0)	T_{1u}^+	$\text{Re } w_{0,0}$
(0,0,1)	A_1^+	$\text{Re } w_{0,0} + \frac{2}{\sqrt{5}} \text{Re } w_{2,0}$
	E^+	$\text{Re } w_{0,0} - \frac{1}{\sqrt{5}} \text{Re } w_{2,0}$
(0,1,1)	A_1^+	$\text{Re } w_{0,0} + \frac{1}{2\sqrt{5}} \text{Re } w_{2,0} - \sqrt{\frac{6}{5}} \text{Im } w_{2,1} - \sqrt{\frac{3}{10}} \text{Re } w_{2,2},$
	B_1^+	$\text{Re } w_{0,0} - \frac{1}{\sqrt{5}} \text{Re } w_{2,0} + \sqrt{\frac{6}{5}} \text{Re } w_{2,2},$
	B_2^+	$\text{Re } w_{0,0} + \frac{1}{2\sqrt{5}} \text{Re } w_{2,0} + \sqrt{\frac{6}{5}} \text{Im } w_{2,1} - \sqrt{\frac{3}{10}} \text{Re } w_{2,2}$
(1,1,1)	A_1^+	$\text{Re } w_{0,0} + 2\sqrt{\frac{6}{5}} \text{Im } w_{2,2}$
	E^+	$\text{Re } w_{0,0} - \sqrt{\frac{6}{5}} \text{Im } w_{2,2}$

Table 1: Expressions for the P -wave phase shifts $\delta_1(E_{\text{cm}})$ relevant for $I = 1$ $\pi\pi$ scattering for various \mathbf{d} and irreps Λ . The quantities w_{lm} are defined in Eq. (14). The irrep labels are discussed in Ref. [6].

where $\delta_L(E)$ are the familiar scattering phase shifts.

For single-channel $\pi\pi$ scattering, $s_1 = s_2 = 0$, so $S = 0$ and $J = L$, in which case Eq. (7) simplifies to

$$F_{L'm_{L'}; Lm_L}^{(s,\gamma,u)} = \frac{1}{2} \left(\delta_{L'L} \delta_{m_{L'}m_L} + W_{L'm_{L'}; Lm_L} \right), \quad (13)$$

using $\rho_a = 1$ for distinguishable $\pi^+\pi^-$. In the case of P -wave scattering of pions, we focus only on the $L = 1$ phase shift and ignore all δ_L for $L \geq 3$, then expressions for $\cot \delta_1$ for various \mathbf{d} and irreps Λ are easily found and are summarized in Table 1, defining

$$w_{lm} = \frac{\mathcal{Z}_{lm}(\mathbf{s}, \gamma, u^2)}{\gamma \pi^{3/2} u^{l+1}}. \quad (14)$$

5 Finite-volume $\pi\pi$ $I = 1$ energies

At rest, the ρ meson appears in the T_{1u}^+ channel, but for nonzero total momenta, we use results in Ref. [6] to determine which little groups contain the ρ . We find that the ρ will appear in the irreps A_1^+ and E^+ of C_{4v} for on-axis total momenta, in the A_1^+ , B_1^+ and B_2^+ irreps of C_{2v} for planar-diagonal momenta, and A_1^+ and E^+ irreps of C_{3v} for cubic-diagonal momenta. The spectrum of energies from each of these channels can be used to compute the $I = 1$ $\pi\pi$ P -wave scattering phase shift, and hence, determine the mass and width of the ρ resonance.

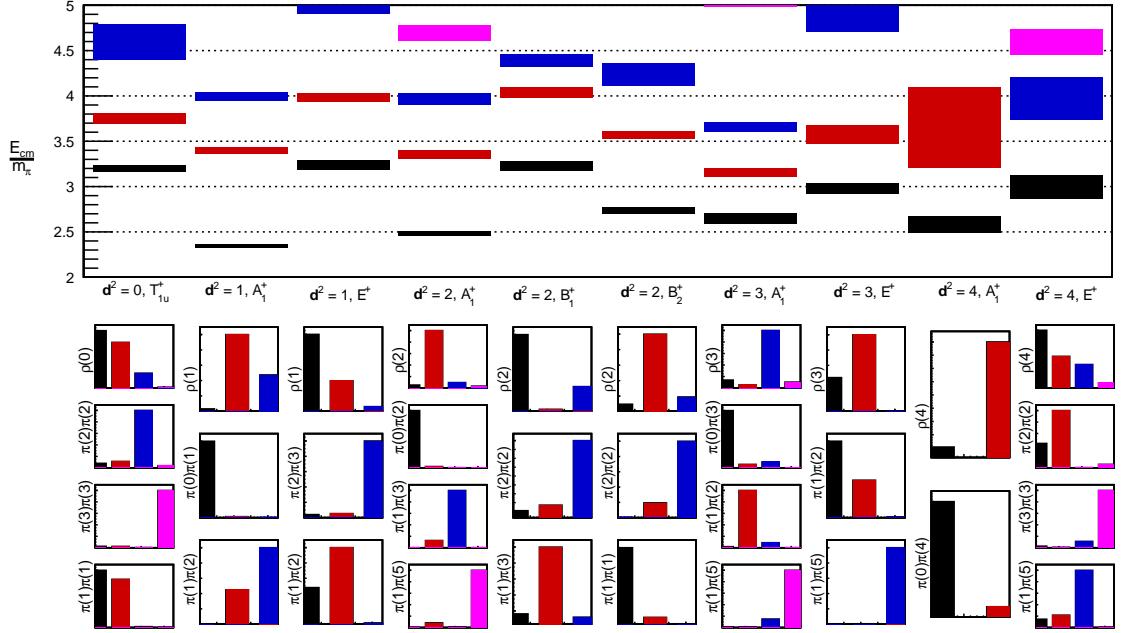


Figure 5: Center-of-mass energies E_{cm}/m_π of ρ and $\pi\pi$ states for various d^2 for each irrep (upper panel), together with the overlaps associated with each interpolating operator (lower panel).

In determining the $\pi\pi$ scattering phase shifts, only energy levels below the inelastic thresholds can be used. In each of the above channels, we include enough two-pion operators of different individual momenta to get a good signal for all states below such thresholds. Fig. 5 shows the energies obtained for the interacting ρ and $\pi\pi$ levels, along with the overlap factors associated with various operators used.

5.1 P -wave scattering phase shifts

To compute the scattering phase shifts using the energies for nonzero total momenta, transformation to the center-of-mass frame is required. Since we are using an anisotropic lattice, energies are measured in terms of the temporal spacing a_t , while the momenta are given in terms of the larger spatial spacing a_s . This means changing frames requires a precise knowledge of the renormalized anisotropy $\xi = a_s/a_t$.

We determine the anisotropy using the dispersion relation of the pion. The energy E of a free particle of mass m and momentum $\mathbf{P} = (2\pi/L)\mathbf{d}$ are related by

$$(a_t E)^2 = (a_t m)^2 + \frac{1}{\xi^2} \left(\frac{2\pi a_s}{L} \right)^2 d^2. \quad (15)$$

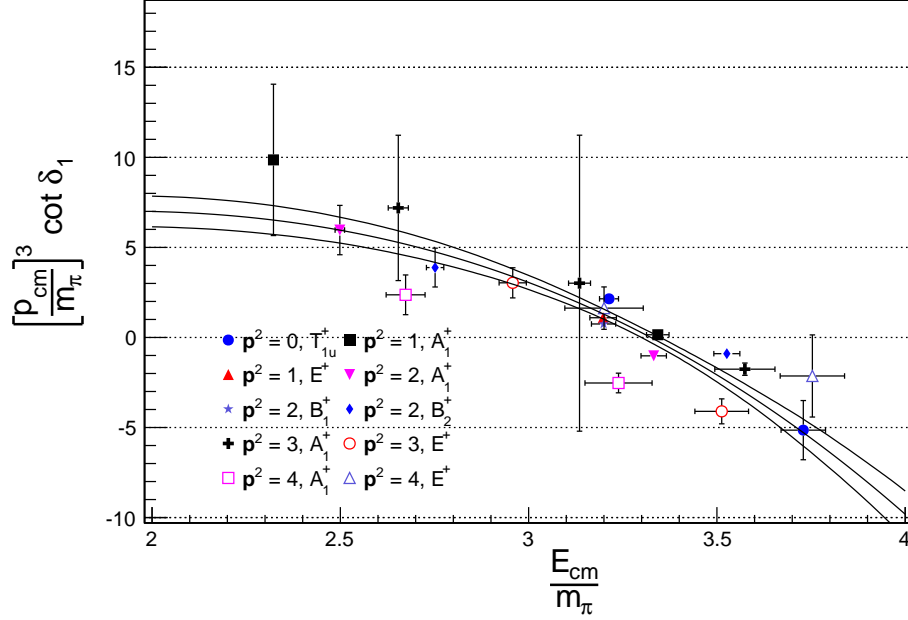


Figure 6: $I = 1$ $\pi\pi$ scattering phase shift $(\mathbf{q}_{\text{cm}}/m_\pi)^3 \cot \delta_1$ against center-of-mass energy E_{cm}/m_π for the anisotropic $32^3 \times 256$ lattice with $m_\pi \approx 240$ MeV.

By evaluating the energies of a particle with different momenta, ξ can be determined.

The energies shown in Fig. 5 were used to compute the δ_1 phase shift using the expressions given in Table 1. Calculating the phase shift requires not only the energy E of a particular state, but also the mass of the pion m_π at rest and the renormalized anisotropy ξ to determine E_{cm} , and hence, \mathbf{q}_{cm} and u . Results were obtained for $\mathbf{q}_{\text{cm}}^3 \cot \delta_1$ and fit to the form

$$g_{\rho\pi\pi}^2 q_{\text{cm}}^3 \cot(\delta_1) = 6\pi E_{\text{cm}}(m_\rho^2 - E_{\text{cm}}^2). \quad (16)$$

Our preliminary results for the $I = 1$ $\pi\pi$ P -wave scattering phase shift are shown in Fig. 6 against the center-of-mass energy E_{cm}/m_π . The width Γ is sensitive to the allowed phase space for its decay products, which depends on the pion mass. Since our pion mass is 240 MeV, we cannot expect our width determination to agree with experiment. However, the effects of phase space can be reduced by writing the width in terms of a coupling $g_{\rho\pi\pi}$:

$$\Gamma(m_r) = \frac{g_{\rho\pi\pi}^2}{48\pi m_r^2} (m_r^2 - 4m_\pi^2)^{3/2}. \quad (17)$$

The coupling $g_{\rho\pi\pi}$ is expected to be fairly insensitive to the quark mass. Our (preliminary) best-fit values for m_ρ and $g_{\rho\pi\pi}$, with errors determined by bootstrap resampling,

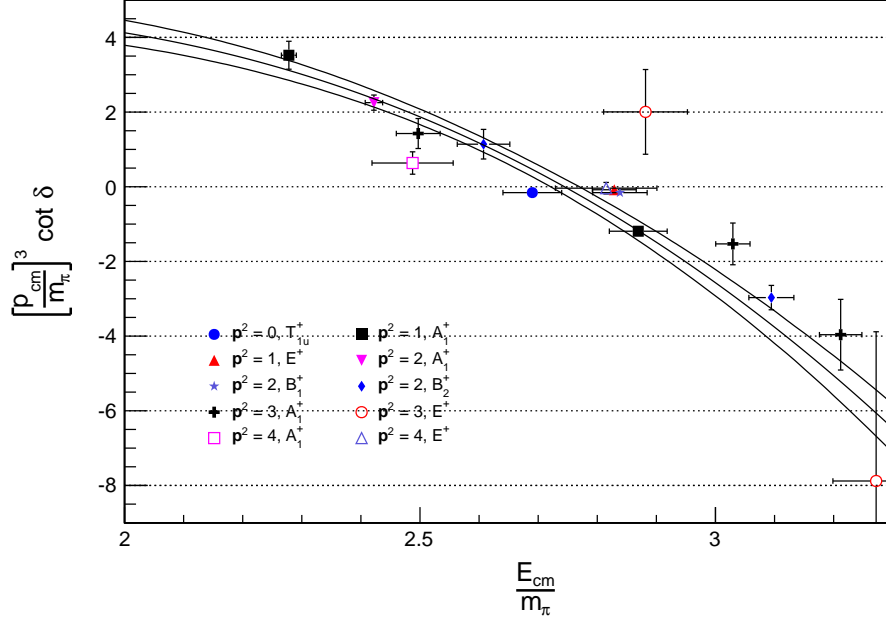


Figure 7: $I = 1$ $\pi\pi$ scattering phase shift $(\mathbf{q}_{\text{cm}}/m_\pi)^3 \cot \delta_1$ against center-of-mass energy E_{cm}/m_π for a $48^3 \times 128$ isotropic lattice with $m_\pi \approx 280$ MeV.

are

$$g_{\rho\pi\pi} = 6.16(36), \quad m_\rho/m_\pi = 3.324(24), \quad \chi^2/\text{dof} = 1.43. \quad (18)$$

These fits are rather complicated. On each bootstrap resampling, a value of $a_t m_\pi$ and ξ must be obtained and used in the fit in order to properly propagate the uncertainty of these two parameters into our determination of $g_{\rho\pi\pi}$ and m_ρ/m_π . A correlated- χ^2 fit must be performed for each bootstrap resampling, which requires evaluating the covariance matrix with an inner bootstrap method. Finally, the model function is not independent of the Monte Carlo data being fit, so the covariance matrix of the residuals must be recalculated every time the model parameters are changed while seeking the best fit! An alternative approach of fitting to the lab frame energies would also have to deal with this issue due to implicit dependence on m_π and ξ .

The results above demonstrate that the stochastic LapH method produces energy estimates of sufficient precision to extract scattering phase shifts. Compared to methods that treat quark propagation exactly, the stochastic LapH method provides a huge reduction in cost and works well even on very large volumes. Preliminary results on a $48^3 \times 128$ isotropic lattice[15] with an improved Wilson gauge and fermion action for $m_\pi \approx 280$ MeV are shown in Fig. 7, yielding best fit values

$$g_{\rho\pi\pi} = 5.68(24), \quad m_\rho/m_\pi = 2.745(24), \quad \chi^2/\text{dof} = 1.20. \quad (19)$$

6 Conclusion

In this talk, our progress in computing the finite-volume stationary-state energies of QCD was described. Our preliminary results in the zero-momentum bosonic $I = 1$, $S = 0$, T_{1u}^+ symmetry sector of QCD on a large $32^3 \times 256$ anisotropic lattice for $m_\pi \sim 240$ MeV using a correlation matrix of 108 operators were presented. All needed Wick contractions were efficiently evaluated using the stochastic LapH method. Issues related to level identification were discussed. Our progress in calculating the $I = 1$ $\pi\pi$ P -wave scattering phase shifts on the $(32^3|240)$ ensemble, as well as a $48^3 \times 128$ isotropic lattice, was also described.

ACKNOWLEDGEMENTS

This work was supported by the U.S. National Science Foundation under awards PHY-1306805 and PHY-1318220, and through the NSF TeraGrid/XSEDE resources provided by TACC and NICS under grant number TG-MCA07S017. B. H. is supported by Science Foundation Ireland under Grant No. 11/RFP/PHY3218.

References

- [1] S. Basak, R.G. Edwards, G.T. Fleming, U.M. Heller, C. Morningstar, D. Richards, I. Sato, S. Wallace, Phys. Rev. D **72**, 094506 (2005).
- [2] S. Basak, R.G. Edwards, G.T. Fleming, K.J. Juge, A. Lichtl, C. Morningstar, D.G. Richards, I. Sato, S.J. Wallace, Phys. Rev. D **76**, 074504 (2007).
- [3] J. Bulava, R.G. Edwards, E. Engelson, J. Foley, B. Joo, A. Lichtl, H.W. Lin, N. Mathur, C. Morningstar, D.G. Richards, S. Wallace, Phys. Rev. D **79**, 034505 (2009).
- [4] J. Bulava, R.G. Edwards, E. Engelson, B. Joo, H-W. Lin, C. Morningstar, D.G. Richards, S.J. Wallace, Phys. Rev. D **82**, 014507 (2010).
- [5] C. Morningstar, J. Bulava, J. Foley, K.J. Juge, D. Lenkner, M. Peardon, C.H. Wong, Phys. Rev. D **83**, 114505 (2011).
- [6] C. Morningstar, J. Bulava, B. Fahy, J. Foley, Y.C. Jhang, K.J. Juge, D. Lenkner, C.H. Wong, Phys. Rev. D **88**, 014511 (2013).
- [7] M. A. Clark, A. D. Kennedy, and Z. Sroczynski, Nucl. Phys. B (Proc. Suppl.) **140**, 835 (2005).

- [8] H.-W. Lin, *et al.*, Phys. Rev. D **79**, 034502 (2009).
- [9] C. Morningstar and M. J. Peardon, Phys. Rev. D **69**, 054501 (2004).
- [10] A. Reifman, B.S. DeWitt, R. Newton, Phys. Rev. **101**, 877 (1956).
- [11] B.S. DeWitt, Phys. Rev. **103**, 1565 (1956).
- [12] M. Lüscher, Nucl. Phys. B **354**, 531 (1991).
- [13] K. Rummukainen, S. Gottlieb, Nucl. Phys. B **450**, 397 (1995).
- [14] C.H. Kim, C.T. Sachrajda, S. Sharpe, Nucl. Phys. B **727**, 218 (2005).
- [15] M. Bruno *et al.*, JHEP **02**, 043 (2015).